IEEE Access
Multidisciplinary | Rapid Review | Open Access Journal

Received February 27, 2018, accepted March 24, 2018, date of publication March 27, 2018, date of current version April 23, 2018.

Digital Object Identifier 10.1109/ACCESS.2018.2820100

Faster-Than-Nyquist Non-Orthogonal Frequency-Division Multiplexing for Visible Light Communications

JI ZHOU[1,2], QI WANG[3], JINLONG WEI[4], QIXIANG CHENG[2], TIANTIAN ZHANG[1], ZHANYU YANG[5], AIYING YANG[6], YUEMING LU[7], AND YAOJUN QIAO[1]

[1]Beijing Key Laboratory of Space-Ground Interconnection and Convergence, School of Information and Communication Engineering, Beijing University of Posts and Telecommunications, Beijing 100876, China
[2]Department of Electrical Engineering, Columbia University, New York, NY 10026, USA
[3]Electronics and Computer Science, University of Southampton, Southampton SO17 1BJ, U.K.
[4]Huawei Düsseldorf GmbH, European Research Center, 80992 München, Germany
[5]Department of Electrical and Computer Engineering, University of Virginia, Charlottesville, VA 22904, USA
[6]School of Optoelectronics, Beijing Institute of Technology, Beijing 100081, China
[7]Key Laboratory of Trustworthy Distributed Computing and Service, Ministry of Education, Beijing University of Posts and Telecommunications, Beijing 100876, China

Corresponding author: Yaojun Qiao (qiao@bupt.edu.cn)

This work was supported in part by the National Natural Science Foundation of China under Grant 61771062 and Grant 61475094, in part by the National Key Research and Development Program under Grant 2016YFB0800302, in part by the BUPT Excellent Ph.D. Students Foundation, and in part by the China Scholarship Council Foundation.

ABSTRACT In this paper, we propose a faster-than-Nyquist non-orthogonal frequency-division multiplexing (NOFDM) scheme for visible light communications (VLCs) where the multiplexing/demultiplexing employs the inverse fractional cosine transform (IFrCT)/FrCT. Different to the common fractional Fourier transform-based NOFDM (FrFT-NOFDM) signal, FrCT-based NOFDM (FrCT-NOFDM) signal is real-valued, which can be directly applied to the VLC systems without the expensive up-conversion and thus it is more suitable for the cost-sensitive VLC systems. Under the same transmission rate, FrCT-NOFDM signal occupies smaller bandwidth compared to OFDM signal. When the bandwidth compression factor α is set to 0.8, 20% bandwidth saving can be obtained. Therefore, FrCT-NOFDM has higher spectral efficiency and suffers less high-frequency distortion compared to OFDM, which benefits the bandwidth-limited VLC systems. As the simulation results show, bit error rate performance of FrCT-NOFDM with α of 0.9 or 0.8 is better than that of OFDM. Meanwhile, FrCT-NOFDM has a superior security performance. In conclusion, FrCT-NOFDM shows the potential for application in the future VLC systems.

INDEX TERMS Faster-than-Nyquist signaling, non-orthogonal frequency-division multiplexing, fractional cosine transform, high spectral efficiency, visible light communications.

I. INTRODUCTION

Recently, visible light communications (VLC) have been proposed to provide high-speed network access for office, shop center, warehouse, and airplane because of many advantages such as the lost-cost front-ends, unregulated huge frequency resources, and no electromagnetic interference [1]–[4]. As a potential access option for the future 5G wireless systems, VLC systems are gaining extensive attention [5]–[7]. However, there are many obstacles for the practical VLC systems. For instance, the data rate of VLC systems is limited by the bandwidth of the light-emitting diodes (LEDs) and multipath effect [8]–[10]. The multipath effect gives rise to the frequency-selective power fading, which seriously limits the effective bandwidth. The longer the delay spread of multipath is, the smaller the effective bandwidth is. How to transmit more data on the limited bandwidth is an important issue in VLC systems.

In order to fully utilize the limited bandwidth of VLC systems, the modulation schemes with high spectral efficiency should be employed. Orthogonal frequency-division multiplexing (OFDM) is a well-known modulation scheme with high spectral efficiency, which has been widely investigated for VLC systems [11]–[15]. As we know, VLC is an intensity-modulation/direct-detection (IM/DD) optical

system. Therefore, OFDM signal for the VLC systems needs to be real-valued and unipolar. For widely-used discrete Fourier transform-based OFDM (DFT-OFDM), Hermitian symmetry should be used to generate the real-valued signal. To obtain the unipolar signal, there are two popular approaches: one is DC-biased optical OFDM (DCO-OFDM) and the other is asymmetrical clipping optical OFDM (ACO-OFDM) [16]–[18]. In DCO-OFDM, the biasing and clipping operations are employed to make the bipolar OFDM signal unipolar. In ACO-OFDM, only the odd subcarriers are valid, whereby the generated bipolar OFDM signal has a redundant negative part. Therefore, an unipolar signal can be obtained by clipping the negative part of the generated bipolar OFDM signal. DCO-OFDM and ACO-OFDM have their respective advantages and disadvantages and thus we can select the suitable one depending on the application scenario.

Non-orthogonal frequency-division multiplexing (NOFDM) systems have been investigated in both wireless and optical communications to further increase the spectral efficiency by compressing the subcarrier spacing [19]–[23]. In conventional NOFDM for IM/DD optical systems, the multiplexing usually employs inverse fractional Fourier transform (IFrFT) [19], [20]. However, the subcarrier distribution in FrFT-based NOFDM (FrFT-NOFDM) is different from that in OFDM, thus the real-valued signal cannot be generated by employing Hermitian symmetry. In general, the upconversion is applied to the complex-valued NOFDM signal for realizing intensity modulation [19], [20]. There are two methods to implement the upconversion: analog and digital methods. In the analog method [19], two-channel digital-to-analog converters (DACs) are required to convert the digital complex-valued NOFDM signal into two analog signals. Then, an in-phase/quadrature (I/Q) mixer with a radio frequency (RF) source is used to combine two analog signals and up-convert to intermediate frequency. The two-channel DACs, I/Q mixer, and RF source are uneconomical for the cost-sensitive VLC systems. In the digital method [20], the upconversion can be implemented by the digital signal processing, which can avoid some expensive analog devices but requires the high-bandwidth DAC. In both analog and digital methods, the generated intermediate-frequency signal has higher bandwidth compared to the baseband signal, which requires the electrical, electro-optic and photoelectric devices with high electrical bandwidth. The high-bandwidth devices are expensive for the cost-sensitive VLC systems.

In 1975, Mazo proposed the first FTN signaling, of which the symbol rate is faster than the Nyquist rate [24], [25]. In our previous work, we proposed the real-valued faster-than-Nyquist (FTN) NOFDM schemes, which have been experimentally demonstrated in the fiber-optic communications [26], [27]. For the IM/DD optical systems, the real-valued FTN NOFDM signal requires no upconversion and has high spectral efficiency. Under the same transmission rate, the real-valued FTN NOFDM signal occupies smaller bandwidth compared to OFDM signal, which is promising in bandwidth-limited VLC systems. In this paper, we apply FTN NOFDM signal to VLC systems and study its performance in detail.

The main contributions of this paper are as follows:

- A novel FTN NOFDM based on fractional cosine transform (FrCT-NOFDM) for VLC systems: The FrCT-NOFDM signal occupies smaller bandwidth than OFDM signal thereby having higher spectral efficiency. Meanwhile, FrCT-NOFDM signal is real-valued. Therefore, it is suitable for the bandwidth-limited and cost-sensitive VLC systems.
- A specific analysis of FrCT-NOFDM system over the optical-wireless channel: The bit error rate (BER) performance of FrCT-NOFDM is comprehensively analyzed under the different bandwidth compression factor, root-mean-square (RMS) delay spread, DC bias, and iterative number. Meanwhile, the simulation result shows that FrCT-NOFDM signal has the potential for application in the security VLC systems owing to the superior security performance.

The rest of this paper is organized as follows. We give the principle of FTN FrCT-NOFDM for the VLC systems in Section II. In Section III, we analyze the optical-wireless channel and noise models for simulation. In Section IV, we implement the simulations and give the simulation results for studying the performance of FrCT-NOFDM in the VLC systems. Finally, the paper is concluded in Section V.

II. PRINCIPLE OF FTN FRCT-NOFDM FOR VLC SYSTEMS

Fig. 1 depicts a block diagram of FTN FrCT-NOFDM for VLC systems. Different from that in FrFT-NOFDM, the multiplexing/demultiplexing processing in FrCT-NOFDM employs the inverse FrCT (IFrCT)/FrCT algorithm, which is defined as

$$x_n = \sqrt{\frac{2}{N}} \sum_{k=0}^{N-1} W_k X_k \cos\left(\frac{\pi\alpha(2n+1)k}{2N}\right), \quad 0 \le n \le N-1, \tag{1}$$

$$X_k = \sqrt{\frac{2}{N}} W_k \sum_{n=0}^{N-1} x_n \cos\left(\frac{\pi\alpha(2n+1)k}{2N}\right), \quad 0 \le k \le N-1 \tag{2}$$

where

$$W_k = \begin{cases} \frac{1}{\sqrt{2}}, & k = 0 \\ 1, & k = 1,\ 2,\ \cdots,\ N-1. \end{cases} \tag{3}$$

The bandwidth compression factor α determines the level of the bandwidth compression. Obviously, IFrCT is a real-valued transform, thus the generated NOFDM signal x_n is real-valued when X_k is real-valued. Therefore, Hermitian symmetry is not required in FrCT-NOFDM for obtaining the real-valued signal. Meanwhile, the upconversion is not required in FrCT-NOFDM for IM/DD optical system.

Figure 2 reveals the sketched spectra of discrete cosine transform (DCT)-based OFDM (DCT-OFDM) (i.e., $\alpha = 1$)

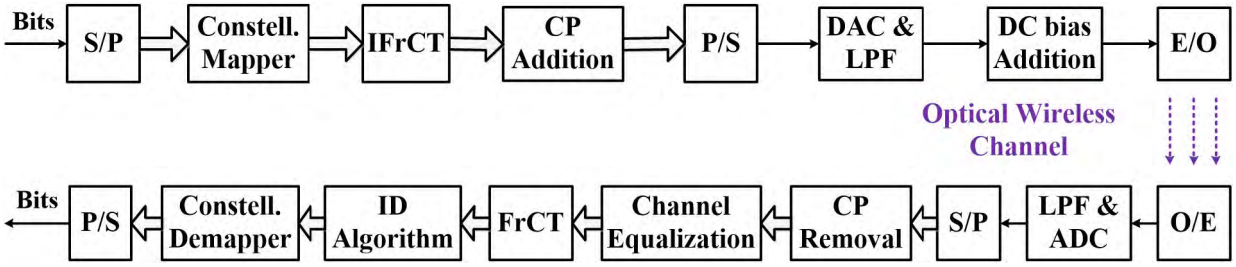

FIGURE 1. Block diagram of FTN FrCT-NOFDM for VLC systems. S/P: series-to-parallel, P/S: parallel-to-series, IFrCT: inverse fractional cosine transform, FrCT: fractional cosine transform, CP: cyclic prefix, DAC: digital-to-analog converter, ADC: analog-to-digital converter, LPF: low-pass filter, E/O: electro/optic, O/E: optic/electro, ID: iterative detection.

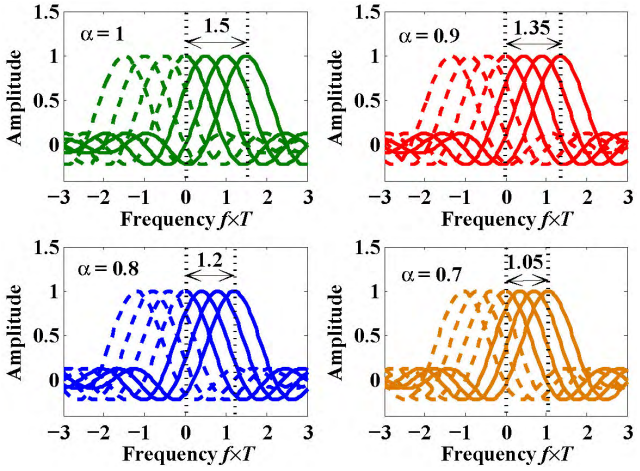

FIGURE 2. Sketched spectra of DCT-OFDM (i.e., $\alpha = 1$) and FrCT-NOFDM when the number of subcarriers is set to 4.

and FrCT-NOFDM when the number of subcarriers is set to 4. The subcarrier spacing of DCT-OFDM is half of that of frequently-used DFT-OFDM, which is equal to $1/2T$ where T denotes the time duration of one symbol [28]–[31]. In DCT-OFDM, all the subcarriers locate on the positive frequency region and their mirror images fall on the negative frequency region [32]–[34]. Due to the compression of subcarrier spacing, the subcarrier spacing of FrCT-NOFDM is expressed as $\alpha/2T$. The bandwidth of FrCT-NOFDM can be calculated by

$$B = \frac{\alpha(N-1)}{2T} + \frac{1}{T} \approx \frac{\alpha N}{2T}. \tag{4}$$

when the subcarrier number is large enough. The bandwidth of FrCT-NOFDM decreases with the decrease of the α. When α is set to 0.8, the bandwidth saving can achieve 20%. Therefore, FrCT-NOFDM has a higher spectral efficiency than DCT-OFDM. As we know, the Nyquist rate is define as the double of bandwidth,

$$R_N = \frac{\alpha N}{T}. \tag{5}$$

The symbol rate of FrCT-NOFDM is equal to

$$R_S = \frac{N}{T}. \tag{6}$$

Therefore, when the α in FrCT-NOFDM is set to 0.8, its symbol rate is 25% faster than its corresponding Nyquist rate.

III. OPTICAL-WIRELESS CHANNEL MODEL AND NOISE MODEL

The optical-wireless channel can be modeled as a linear baseband system. The received signal after optical-wireless channel is defined as

$$r(t) = h(t) * x(t) + n(t) \tag{7}$$

where $h(t)$ is the channel impulse response of optical-wireless channel, $x(t)$ is the transmitted signal, $n(t)$ is the noise component, and $*$ denotes the convolution operation. The $h(t)$ is expressed as

$$h(t) = \sum_{n=0}^{N_D} h_n \delta(t - n\Delta\tau) \tag{8}$$

where N_D is the number of paths, h_n is the channel coefficient and $n\Delta\tau$ is the delay of the n-th path.

In general, the optical-wireless channel models fall into two categories: directed and non-directed (i.e. diffused) models [35]–[37]. In the directed model, line of sight (LOS) plays the major role. Therefore, the directed model can be appropriately considered as an additive white Gaussian noise (AWGN) channel model. In the non-directed model, the optical power propagates along various paths with different lengths, which causes the multipath effect. In this paper, we employ the non-directed model to investigate the influence of the multipath effect on FrCT-NOFDM. The multipath effect is usually caused by two ways: one is the multiple-reflection light and the other is the single-reflection light. The exponential-decay (ED) and ceiling-bounce (CB) models were proposed to model both multiple reflection light and single reflection light [35]. The channel impulse response of the ED model can be defined as

$$h_{ed}(t) = \frac{1}{2D} e^{-\frac{t}{2D}} u(t) \tag{9}$$

where the D is the RMS delay spread of the multiple reflections and $u(t)$ is the unit step function. The channel impulse response of the CB model is given by

$$h_{cb}(t) = \frac{6a^6}{(t+a)^7} u(t) \tag{10}$$

where $a = 12\sqrt{\frac{11}{13}}D$.

Figure 3 shows the transfer function of the ED and CB models. In our simulation, the RMS delay spread is set to the values from 1.5 ns to 9 ns [41]. When the RMS delay spread is set to 1.5 ns, the 3-dB bandwidth of ED model and CB model is 33.7 MHz and 31.4 MHz, respectively. Therefore, the 3-dB bandwidth of the ED model is slightly wider than that of the CB model for the same RMS delay spread. When the RMS delay spread is set to 3 ns, 6 ns, and 9 ns, the 3-dB bandwidth of the CB model is 20.9 MHz, 11.7 MHz, and 8.3 MHz, respectively. The 3-dB bandwidth of the CB model decreases with the increase of the RMS delay spread. The multipath effect causes the frequency-selective power fading, which seriously limits the effective bandwidth. For VLC systems, there are many other complex channel models, which are derived from the non-directed model by considering many other conditions such as the position of LED and photodiode (PD) and the field of view of the PD [38]–[40]. In this paper, we aim to investigate the performance of FrCT-NOFDM signal influenced by the multipath effect. Without loss of generality, we can employ the CB model to achieve the aim in the simulation. In optical-wireless systems, there are two main noise components: receiver circuit thermal noise and photon noise, which are subject to the white Gaussian distribution and both independent of the transmitted signal [36], [37]. Therefore, we can model the total noise $n(t)$ as the Gaussian and signal-independent distribution in the simulation.

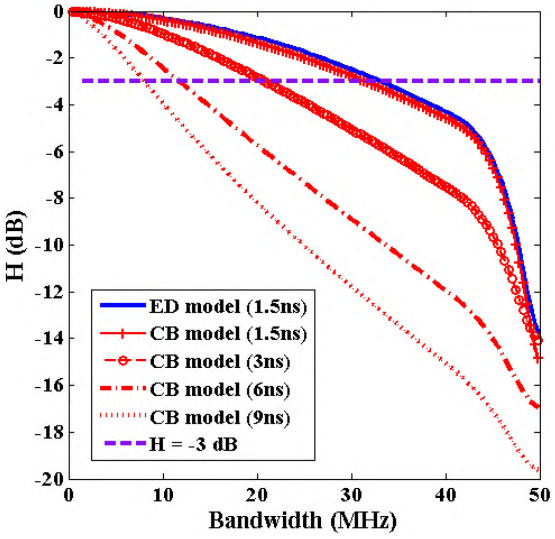

FIGURE 3. The transfer function of the exponential-decay (ED) and ceiling-bounce (CB) models.

IV. SIMULATION SETUP AND RESULTS

A. SIMULATION SETUP

In this section, we present the simulation setup and the detail of channel equalization and inter-carrier interference (ICI) cancellation algorithm.

For VLC systems, the simulation of FrCT-NOFDM is implemented by MATLAB based on the block diagram shown in Fig. 1. The encoding block mainly consists of the real constellation mapper, 256-point IFrCT, and cyclic prefix (CP) addition. In our simulation, the modulated constellation employs the 2-PAM. For resisting the inter-symbol interference, the CP length is set to 1/16 of the symbol duration in FrCT-NOFDM by simultaneously considering the performance and spectral efficiency. In one frame, 256 FrCT-NOFDM symbols and 10 training symbols are transmitted. Eight frames are used to calculate the BER. A suitable DC bias is required to make the FrCT-NOFDM signal to be unipolar. The transmission rate of the generated FrCT-NOFDM signal is set to 100 Mbit/s.

As shown in Section III, the optical-wireless channel employs the CB model and the adding noise is Gaussian and signal-independent in the simulation. Fig. 4 shows the spectra for the DCT-OFDM and FrCT-NOFDM signals with the transmission rate of 100 Mbit/s after the optical-wireless channel. The dark line denotes the transfer function of CB model with 3-ns RMS delay spread. After the optical-wireless channel, the signals suffer the high-frequency distortion. The bandwidth of 100-Mbit/s DCT-OFDM signal is equal to 50 MHz, which is half of the transmission rate. The bandwidth of FrCT-NOFDM signal is smaller than that of DCT-OFDM, which is 45 MHz, 40 MHz, and 35 MHz when the α is set to 0.9, 0.8, and 0.7, respectively. Therefore, FrCT-NOFDM occupies smaller bandwidth and thus achieves higher spectral efficiency compared to DCT-OFDM.

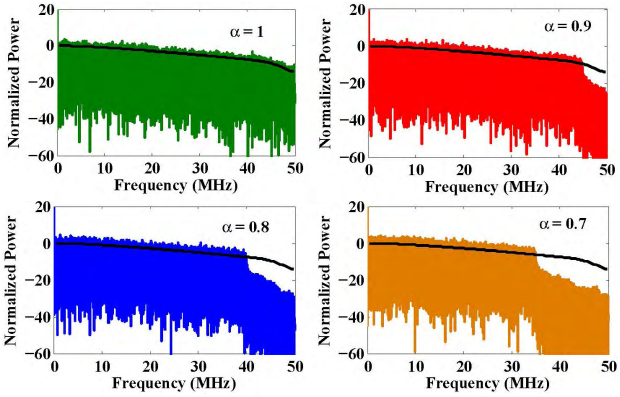

FIGURE 4. The spectra for DCT-OFDM and FrCT-NOFDM signals with transmission rate of 100 Mbit/s after the optical-wireless channel. The dark line denotes the transfer function of the CB model with 3-ns RMS delay spread.

The decoding block mainly consists of CP removal, channel equalization, 256-point FrCT, iterative detection (ID) algorithm, and constellation demapper. The channel estimation and frequency-domain equalization are implemented to compensate the channel distortion. The non-orthogonal subcarriers give rise to ICI, which seriously deteriorates the BER performance. The ICI is able to be eliminated by the ID algorithm.

Figure 5 depicts the block diagram of channel estimation and frequency-domain equalization for FrCT-NOFDM. In the channel estimation, the channel characteristic can be estimated by the training symbols. The received training symbols are sent to the DFT module to obtain its frequency-domain symbols $\boldsymbol{T}'$. The channel matrix $\boldsymbol{H}$ can be calculated

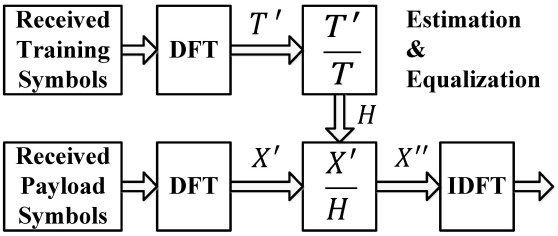

FIGURE 5. Block diagram of channel estimation and frequency-domain equalization for FrCT-NOFDM.

by $\boldsymbol{T}'/\boldsymbol{T}$ where $\boldsymbol{T}$ are the transmitted training symbols in the frequency domain. In the frequency-domain equalization, the received payload symbols are firstly transformed from the time domain into the frequency domain. The frequency-domain payload symbols $\boldsymbol{X}'$ are divided by the channel matrix $\boldsymbol{H}$ to realize the equalization. After equalization, the output symbols $\boldsymbol{X}''$ are sent to IDFT module. The outputs of IDFT module are the FrCT-NOFDM symbols after equalization.

Algorithm 1 depicts the detailed processing of the ID algorithm for 2-PAM-modulated FrCT-NOFDM. The correlation matrix $\mathbf{C}$ can be calculated by,

$$C_{l,m} = \frac{2W_l W_m}{N} \sum_{k=0}^{N-1} \cos\left(\frac{\alpha\pi l(2k+1)}{2N}\right)\cos\left(\frac{\alpha\pi(2k+1)m}{2N}\right), \tag{11}$$

which represents the interference between l-th and m-th subcarriers.

Algorithm 1 ID Algorithm for FrCT-NOFDM

Input: Received symbol : $\mathbf{R}$; Correlation matrix : $\mathbf{C}$; Iterative number : I; Identity matrix : $\mathbf{e}$.
Output: Recovered symbol : $\mathbf{S}$.

```
Initialization : S_0 = 0, d = 1                ▷ Beginning of iteration
for i = 1; i ≤ I; i++ do
    S_i = R − (C − e)S_{i−1}                   ▷ Eliminating the ICI
    if S_i > d then                            ▷ Signal decision
        S_i = 1
    else if S_i < −d then
        S_i = −1
    else
        S_i = S_i
    end if
    d = 1 − i/I                                ▷ Updating d
end for
S = S_I
Return S
```

The ID algorithm can be implemented by three steps. The first step reduces the ICI by

$$\mathbf{S}_i = \mathbf{R} - (\mathbf{C} - \mathbf{e})\mathbf{S}_{i-1} \tag{12}$$

where i denotes the i-th iteration. The second step is the decision operation. The signals falling on the decision regions (i.e., the value of the signal is larger than d or smaller than $-d$) can be mapped into the desired constellation points. The last step is updating the decision level by $d = 1 - i/I$ where I is the total iterative number. Finally, the recovered symbol $\mathbf{S}$ can be obtained after the I-th iteration.

B. SIMULATION RESULTS

In this section, we give the simulation results of FrCT-NOFDM for the VLC systems. The BER performance of FrCT-NOFDM is comprehensively analyzed under different α, RMS delay spread, DC bias, and iterative number. Meanwhile, FrCT-NOFDM shows a superior security performance.

Figure 6 shows BER versus the SNR for DCT-OFDM and FrCT-NOFDM signals. The RMS delay spread is set to 3 ns, the DC bias is set to 7 dB, and the iterative number of ID algorithm is set to 20. In FrCT-NOFDM with α of 0.9 or 0.8, the BER can achieve the 7% forward error correction (FEC) limit (i.e., the BER of 3.8×10^{-3}) at the SNR of $\sim$ 22 dB. In DCT-OFDM, the BER can achieve the 7% FEC limit at the SNR of $\sim$ 24.2 dB. When α is set to 0.9 or 0.8, FrCT-NOFDM exhibits an improvement in the SNR of $\sim$ 2.2 dB compared to DCT-OFDM. As Fig. 4 shows, the power of high-frequency part in DCT-OFDM signal is seriously declined, but the high-frequency part in FrCT-NOFDM is empty owing to the bandwidth compression. Therefore, DCT-OFDM suffers more high-frequency distortion and has worse BER performance compared to FrCT-NOFDM with α of 0.9 or 0.8.

In FrCT-NOFDM, the residual ICI after ID algorithm increases with the decrease of α. As Fig. 6 depicts, when the SNR is larger than 22 dB, the BER performance of FrCT-NOFDM with α of 0.8 become worse than that of FrCT-NOFDM with α of 0.9. This is because the residual ICI in FrCT-NOFDM with α of 0.8 is larger than that in FrCT-NOFDM with α of 0.9, and with the increase of SNR, the residual ICI turns into the major distortion. Due to the large residual ICI, FrCT-NOFDM with α of 0.7 can not achieve the 7% FEC limit at the SNR of 30 dB.

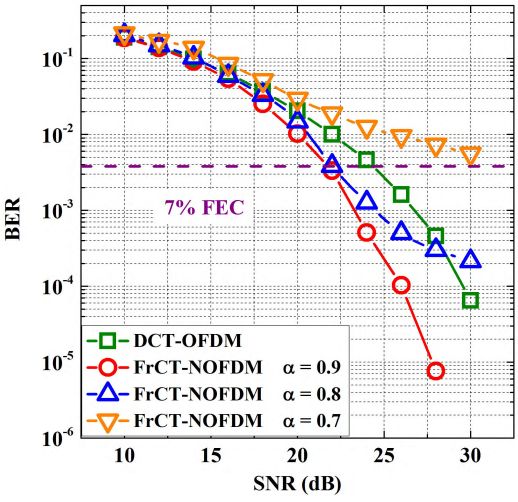

FIGURE 6. BER versus the SNR for DCT-OFDM and FrCT-NOFDM signals.

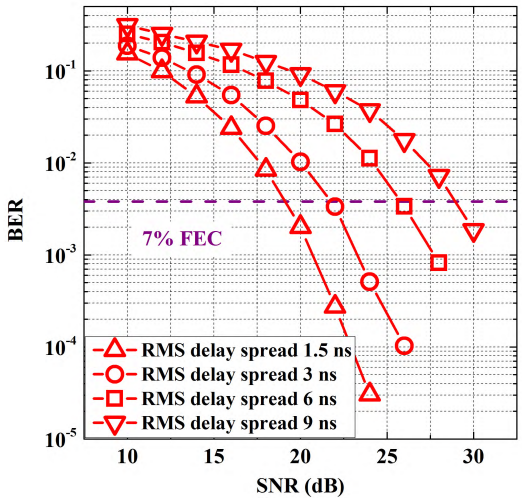

FIGURE 7. BER against the SNR for different RMS delay spread of the optical-wireless channel.

Figure 7 reveals the BER against the SNR for different RMS delay spread of the optical-wireless channel. The α of FrCT-NOFDM is set to 0.9, the DC bias is set to 7 dB and the iterative number of ID algorithm is set to 20. The BER performance deteriorates with the increase of the RMS delay spread due to the decrease of the channel bandwidth. When RMS delay spread is set to 9 ns, the bandwidth of the CB model is only 8.3 MHz, which is insufficient for the signal with 45-MHz bandwidth. Under this condition, BER can only achieve the 7% FEC limit under the SNR of 30 dB.

Figure 8 depicts the required SNR at the 7% FEC limit against the RMS delay spread for DCT-OFDM and FrCT-NOFDM with α of 0.9. When RMS delay spread is set to 1.5 ns, the required SNR for DCT-OFDM signal is about 4.4-dB higher than that for FrCT-NOFDM signal. As shown in Fig. 3, when the RMS delay spread is set to 1.5 ns,

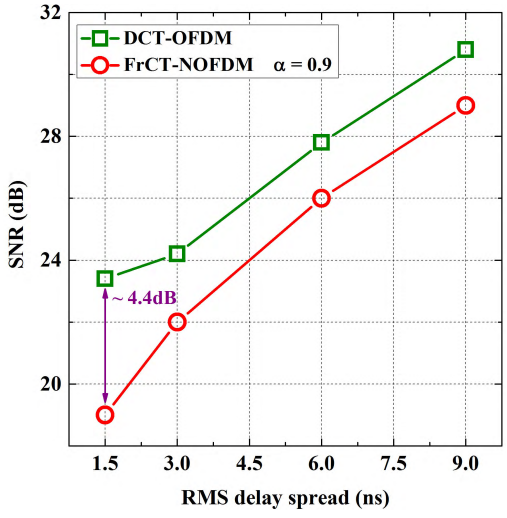

FIGURE 8. The required SNR at the 7% FEC limit against the RMS delay spread for DCT-OFDM signal and FrCT-NOFDM signal with α of 0.9.

the transfer function of the CB model is fading fast while the bandwidth is larger than 45 MHz, looking like a cliff. This fast high-frequency power fading seriously degrades the performance of the subcarriers between 45 MHz and 50 MHz in DCT-OFDM. However, there is no subcarrier between 45 MHz and 50 MHz in FrCT-NOFDM with α of 0.9, thus it is almost not influenced by that fast high-frequency power fading. When RMS delay spread increases, the high-frequency power fading becomes smooth. Therefore, the difference of the required SNR between DCT-OFDM and FrCT-NOFDM is no longer so large. The required SNR in FrCT-NOFDM is approximately 2 dB smaller than that in DCT-OFDM when RMS delay spread is equal or greater than 3 ns.

Figure 9 shows the BER versus the SNR for different DC bias in FrCT-NOFDM when α is set to 0.9. The iterative number of ID algorithm is set to 20 and the RMS delay spread is set to 3 ns. In IM/DD VLC systems, FrCT-NOFDM suffers the clipping distortion, which decreases with the increase of DC bias. If the DC bias is large enough, there is almost no clipping noise in FrCT-NOFDM and its power is approximately equal to the power of useful signal plus the power of DC bias. Therefore, when the DC bias is large enough, the difference between the required SNRs for FrCT-NOFDM with different DC bias is equal to the difference between the corresponding DC-bias power. When the DC bias is 4 dB, the signal still suffers the clipping noise, thus the difference between the required SNRs of FrCT-NOFDM with 4- and 7-dB DC bias is smaller than 3 dB. However, when DC bias is larger than 7 dB, there is little clipping noise in the signal. The difference between the required SNRs of FrCT-NOFDM with 7- and 10-dB DC bias is almost equal to 3 dB. The simulation result coincides with the theoretical analysis.

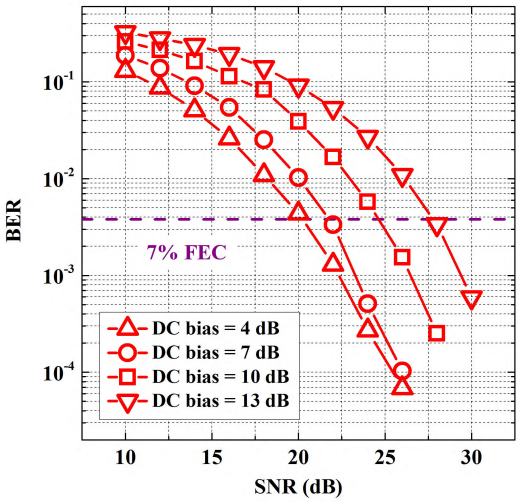

FIGURE 9. BER versus the SNR for different DC bias in FrCT-NOFDM signal when α is set to 0.9.

Figure 10 shows the BER against the SNR for different iterative numbers of the ID algorithm. The α of FrCT-NOFDM is set to 0.8, the RMS delay spread is set to 3 ns, and the DC bias is set to 7 dB. When the ID algorithm is

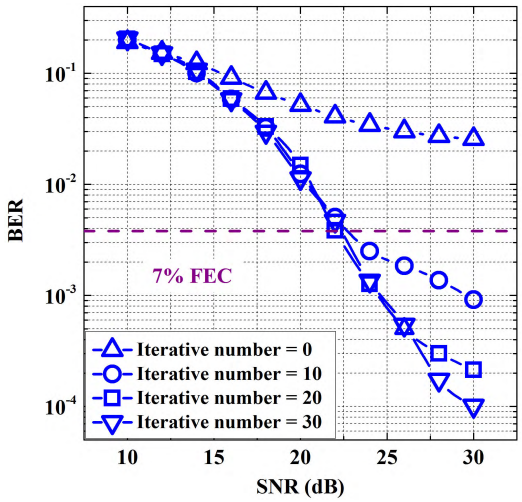

FIGURE 10. BER against the SNR for different iterative numbers of the ID algorithm when the α is set to 0.8 in FrCT-NOFDM.

not employed (i.e., the iterative number is set to 0), the BER cannot achieve the 7% FEC limit although the SNR is set to 30 dB. This is because the ICI seriously degrades the BER performance of FrCT-NOFDM. With the increase of the iterative number, the BER performance is markedly improved. Therefore, the ICI can be effectively eliminated by ID algorithm. However, the complexity of ID algorithm increases with the iterative number. The performance of ID algorithm will no longer be obviously improved with the increase of the iterative number while the iterative number is large. Therefore, we can choose the suitable iterative number by synthetically considering the effect and complexity of ID algorithm.

Figure 11 shows the BER versus $\Delta\alpha$ for FrCT-NOFDM signal when α at the transmitter is set to 0.9 and SNR is set to 28 dB. The iterative number of ID algorithm is set to 20 and

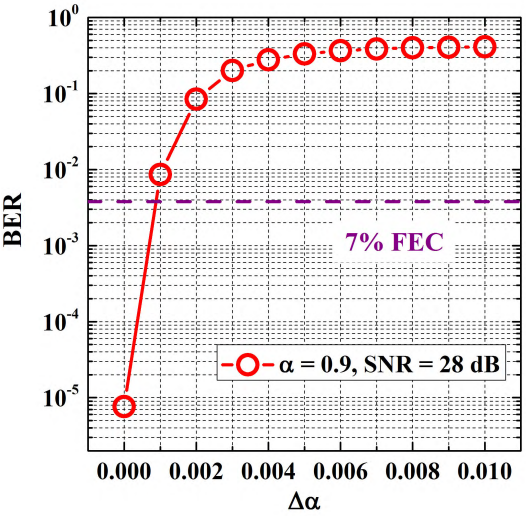

FIGURE 11. BER versus $\Delta\alpha$ for FrCT-NOFDM signal when α at the transmitter is set to 0.9 and SNR is set to 28 dB.

the RMS delay spread is set to 3 ns. The $\Delta\alpha$ denotes the deviation of α between the transmitter and receiver. When $\Delta\alpha$ is larger than 0.001, the BER performance will be significantly deteriorated (BER $>$ 7% FEC limit). In other words, the data can only be recovered accurately when $\Delta\alpha$ is less than 0.001. This is because both FrCT and ID algorithm at the receiver need an accurate α. Therefore, α can be used as an encryption key for the security communications. If the α can not be known accurately, the transmitted data cannot be accurately recovered at the receiver. It reveals that FrCT-NOFDM signal has the superior security performance for application in the security VLC systems.

V. CONCLUSION

This paper proposed the FTN FrCT-NOFDM signal for VLC systems. Compared to FrFT-NOFDM signal, FrCT-NOFDM signal is real-valued, which can be directly applied to the VLC systems without upconversion. Therefore, FrCT-NOFDM signal is more suitable for cost-sensitive VLC systems. Under the same transmission rate, FrCT-NOFDM signal occupies smaller bandwidth compared to OFDM signal. When α is set to 0.8, 20% bandwidth saving can be obtained. By this way, FrCT-NOFDM signal suffers less high-frequency distortion, which is suited to the bandwidth-limited VLC systems.

We presented the simulations to investigate the performance of FrCT-NOFDM. When the RMS delay spread is set to 3 ns (i.e., the 3-dB channel bandwidth is 20.9 MHz) and the transmission rate is set to 100 Mbit/s, FrCT-NOFDM with α of 0.9 or 0.8 exhibits an improvement in the SNR of 2.2 dB compared to DCT-OFDM because of the less high-frequency distortion. Meanwhile, FrCT-NOFDM has the superior security performance for application in the security VLC systems. However, it is worth noting that the residual ICI after ID algorithm is still a critical problem for the high-order constellations and thus the more effective algorithm will be investigated to solve this problem in our future work, such as the simplified maximum likelihood detection [42]–[44]. In conclusion, FrCT-NOFDM shows the potential for application in the future VLC systems.

REFERENCES

[1] M. Biagi, S. Pergoloni, and A. Vegni, "LAST: A framework to localize, access, schedule, and transmit in indoor VLC systems," *J. Lightw. Technol.*, vol. 33, no. 9, pp. 1872–1887, May 1, 2015.

[2] H. Elgala, R. Mesleh, and H. Haas, "Indoor optical wireless communication: Potential and state-of-the-art," *IEEE Commun. Mag.*, vol. 49, no. 9, pp. 56–62, Sep. 2011.

[3] T. R. Gross, S. Mangold, and S. Schmid, "Software-centric VLC networking for the IoT," in *Proc. IEEE Photon. Soc. Summer Topical Meeting Ser.*, Newport Beach, CA, USA, Jul. 2016, pp. 62–63.

[4] N. Chi, H. Haas, M. Kavehrad, T. D. C. Little, and X.-L. Huang, "Visible light communications: Demand factors, benefits and opportunities [Guest Editorial]," *IEEE Wireless Commun.*, vol. 22, no. 2, pp. 5–7, Apr. 2015.

[5] S. Wu, H. Wang, and C. H. Youn, "Visible light communications for 5G wireless networking systems: From fixed to mobile communications," *IEEE Netw.*, vol. 28, no. 6, pp. 41–45, Nov. 2014.

[6] M. B. Rahaim and T. D. C. Little, "Toward practical integration of dual-use VLC within 5G networks," *IEEE Wireless Commun.*, vol. 22, no. 4, pp. 97–103, Aug. 2015.

[7] M. Ayyash *et al.*, "Coexistence of WiFi and LiFi toward 5G: Concepts, opportunities, and challenges," *IEEE Commun. Mag.*, vol. 54, no. 2, pp. 64–71, Feb. 2016.
[8] Z. Ghassemlooy, S. Arnon, M. Uysal, Z. Xu, and J. Cheng, "Emerging optical wireless communications-advances and challenges," *IEEE J. Sel. Areas Commun.*, vol. 33, no. 9, pp. 1738–1749, Sep. 2015.
[9] N. Chi, Y. Wang, Y. Wang, X. Huang, and X. Lu, "Ultra-high-speed single red-green-blue light-emitting diode-based visible light communication system utilizing advanced modulation formats," *Chin. Opt. Lett.*, vol. 12, no. 1, pp. 010605-1–010605-4, Jan. 2014.
[10] M. Biagi, T. Borogovac, and T. D. C. Little, "Adaptive receiver for indoor visible light communications," *J. Lightw. Technol.*, vol. 31, no. 23, pp. 3676–3686, Dec. 1, 2013.
[11] D. Tsonev, S. Videv, and H. Haas, "Unlocking spectral efficiency in intensity modulation and direct detection systems," *IEEE J. Sel. Areas Commun.*, vol. 33, no. 9, pp. 1758–1770, Sep. 2015.
[12] H. Elgala and T. D. C. Little, "SEE-OFDM: Spectral and energy efficient OFDM for optical IM/DD systems," in *Proc. IEEE 25th Annu. Int. Symp. Pers., Indoor, Mobile Radio Commun.*, Washington, DC, USA, Sep. 2014, pp. 851–855.
[13] Q. Wang, C. Qian, X. Guo, Z. Wang, D. G. Cunningham, and I. H. White, "Layered ACO-OFDM for intensity-modulated direct-detection optical wireless transmission," *Opt. Exp.*, vol. 23, no. 9, pp. 12382–12393, May 2015.
[14] Q. Wang, Z. Wang, and L. Dai, "Asymmetrical hybrid optical OFDM for visible light communications with dimming control," *IEEE Photon. Technol. Lett.*, vol. 27, no. 9, pp. 974–977, May 1, 2015.
[15] M. S. A. Mossaad, S. Hranilovic, and L. Lampe, "Visible light communications using OFDM and multiple LEDs," *IEEE Trans. Commun.*, vol. 63, no. 11, pp. 4304–4313, Nov. 2015.
[16] J. Armstrong and B. Schmidt, "Comparison of asymmetrically clipped optical OFDM and DC-biased optical OFDM in AWGN," *IEEE Commun. Lett.*, vol. 12, no. 5, pp. 343–345, May 2008.
[17] S. D. Dissanayake and J. Armstrong, "Comparison of ACO-OFDM, DCO-OFDM and ADO-OFDM in IM/DD systems," *J. Lightw. Technol.*, vol. 31, no. 7, pp. 1063–1072, Apr. 1, 2013.
[18] J. Zhou, Y. Yan, Z. Cai, Y. Qiao, and Y. Ji, "A cost-effective and efficient scheme for optical OFDM in short-range IM/DD systems," *IEEE Photon. Technol. Lett.*, vol. 26, no. 13, pp. 1372–1374, Jul. 1, 2014.
[19] I. Darwazeh, T. Xu, T. Gui, Y. Bao, and Z. Li, "Optical SEFDM system; bandwidth saving using non-orthogonal sub-carriers," *IEEE Photon. Technol. Lett.*, vol. 26, no. 4, pp. 352–355, Feb. 15, 2013.
[20] Y. Wang *et al.*, "SEFDM based spectrum compressed VLC system using RLS time-domain channel estimation and ID-FSD hybrid decoder," in *Proc. 42nd Eur. Conf. Exhibit. Opt. Commun.*, Düsseldorf, Germany, Sep. 2016, pp. 827–829.
[21] Y. Wang *et al.*, "Efficient MMSE-SQRD-based MIMO decoder for SEFDM-based 2.4-Gb/s-spectrum-compressed WDM VLC system," *IEEE Photon. J.*, vol. 8, no. 4, Jul. 2016, Art. no. 7905709.
[22] T. Xu and I. Darwazeh, "A soft detector for spectrally efficient systems with non-orthogonal overlapped sub-carriers," *IEEE Commun. Lett.*, vol. 18, no. 10, pp. 1847–1850, Oct. 2014.
[23] D. Nopchinda, T. Xu, R. Maher, B. C. Thomsen, and I. Darwazeh, "Dual polarization coherent optical spectrally efficient frequency division multiplexing," *IEEE Photon. Technol. Lett.*, vol. 28, no. 1, pp. 83–86, Jan. 1, 2016.
[24] J. E. Mazo, "Faster-than-Nyquist signaling," *Bell Syst. Tech. J.*, vol. 54, no. 8, pp. 1451–1462, Oct. 1975.
[25] J. B. Anderson, F. Rusek, and V. Öwall, "Faster-than-Nyquist signaling," *Proc. IEEE*, vol. 101, no. 8, pp. 1817–1830, Aug. 2013.
[26] J. Zhou, Y. Qiao, Z. Yang, and E. Sun, "Faster-than-Nyquist non-orthogonal frequency-division multiplexing based on fractional Hartley transform," *Opt. Lett.*, vol. 41, no. 19, pp. 4488–4491, Oct. 2016.
[27] J. Zhou *et al.*, "Capacity limit for faster-than-Nyquist non-orthogonal frequency-division multiplexing signaling," *Sci. Rep.*, vol. 7, Jun. 2017, Art. no. 3380.
[28] P. Tan and N. C. Beaulieu, "A comparison of DCT-based OFDM and DFT-based OFDM in frequency offset and fading channels," *IEEE Trans. Commun.*, vol. 54, no. 11, pp. 2113–2125, Nov. 2006.
[29] J. Zhao and A. D. Ellis, "A novel optical fast OFDM with reduced channel spacing equal to half of the symbol rate per carrier," in *Proc. Opt. Fiber Commun., Nat. Fiber Opt. Eng. Conf.*, San Diego, CA, USA, Mar. 2010, pp. 1–3, paper OMR1.
[30] E. Giacoumidis, S. K. Ibrahim, J. Zhao, J. M. Tang, I. Tomkos, and A. D. Ellis, "Experimental demonstration of cost-effective intensity-modulation and direct-detection optical fast-OFDM over 40 km SMF transmission," in *Proc. Opt. Fiber Commun. Conf. Expo., Nat. Fiber Opt. Eng. Conf.*, Los Angeles, CA, USA, Mar. 2012, pp. 1–3, paper JW2A.65.
[31] E. Giacoumidis *et al.*, "Extensive comparisons of optical fast-OFDM and conventional optical OFDM for local and access networks," *J. Opt. Commun. Netw.*, vol. 4, no. 10, pp. 724–733, Oct. 2012.
[32] X. Ouyang and J. Zhao, "Single-tap equalization for fast OFDM signals under generic linear channels," *IEEE Commun. Lett.*, vol. 18, no. 8, pp. 1319–1322, Aug. 2014.
[33] J. Zhou, Y. Qiao, Z. Cai, and Y. Ji, "Asymmetrically clipped optical fast OFDM based on discrete cosine transform for IM/DD systems," *J. Lightw. Technol.*, vol. 33, no. 9, pp. 1920–1927, May 1, 2015.
[34] J. Zhou *et al.*, "FOFDM based on discrete cosine transform for intensity-modulated and direct-detected systems," *J. Lightw. Technol.*, vol. 34, no. 16, pp. 3717–3725, Aug. 15, 2016.
[35] J. B. Carruthers and J. M. Kahn, "Modeling of nondirected wireless infrared channels," *IEEE Trans. Commun.*, vol. 45, no. 10, pp. 1260–1268, Oct. 1997.
[36] J. M. Kahn and J. R. Barry, "Wireless infrared communications," *Proc. IEEE*, vol. 85, no. 2, pp. 265–298, Feb. 1997.
[37] V. Jungnickel, V. Pohl, S. Nonnig, and C. V. Helmolt, "A physical model of the wireless infrared communication channel," *IEEE J. Sel. Areas Commun.*, vol. 20, no. 3, pp. 631–640, Apr. 2002.
[38] C. Chen, D. Basnayaka, and H. Haas, "Non-line-of-sight channel impulse response characterisation in visible light communications," in *Proc. IEEE Int. Conf. Commun. (ICC)*, Kuala Lumpur, Malaysia, May 2016, pp. 1–6.
[39] P. Chvojka, S. Zvanovec, P. A. Haigh, and Z. Ghassemlooy, "Channel characteristics of visible light communications within dynamic indoor environment," *IEEE J. Lightw. Technol.*, vol. 33, no. 9, pp. 1719–1725, May 1, 2015.
[40] K. Lee, H. Park, and J. R. Barry, "Indoor channel characteristics for visible light communications," *IEEE Commun. Lett.*, vol. 15, no. 2, pp. 217–219, Feb. 2011.
[41] F. Miramirkhani and M. Uysal, "Channel modeling and characterization for visible light communications," *IEEE Photon. J.*, vol. 7, no. 6, Dec. 2015, Art. no. 7905616.
[42] M. Imani and U.M. Braga-Neto, "Maximum-likelihood adaptive filtering for partially-observed boolean dynamical systems," *IEEE Trans. Signal Process.*, vol. 65, no. 2, pp. 359–371, Jan. 2017.
[43] R. W. Heath, N. Gonzalez-Prelcic, S. Rangan, W. Roh, and A. M. Sayeed, "An overview of signal processing techniques for millimeter wave MIMO systems," *IEEE J. Sel. Topics Signal Process.*, vol. 10, no. 3, pp. 436–453, Apr. 2016.
[44] L. D. McClenny, M. Imani, and U. M. Braga-Neto, "Boolean Kalman Filter with correlated observation noise," in *Proc. IEEE Int. Conf. Acoust., Speech Signal Process. (ICASSP)*, New Orleans, LA, USA, Mar. 2017, pp. 866–870.

JI ZHOU received the B.S. degree in communication engineering from the Beijing University of Posts and Telecommunications, China, in 2012, where he is currently pursuing the Ph.D. degree with the School of Information and Communication Engineering. His research interests include modulation and signal processing for optical and wireless communications.

QI WANG received the B.E. degree and the Ph.D. degree (Hons.) in electronic engineering from Tsinghua University, Beijing, China, in 2011 and 2016, respectively. From 2014 to 2015, he was a Visiting Scholar with the Electrical Engineering Division, Centre for Photonic Systems, Department of Engineering, University of Cambridge. Since 2016, he has been a Research Fellow with the Southampton Wireless Group, University of Southampton, Southampton, U.K. He has authored over 20 IEEE/OSA journal papers and several conference papers. His research interests include modulation and signal processing for wireless communication and visible light communication. He serves as a TPC Member for many IEEE conferences, including GLOBECOM, GlobalSIP, CSNDSP, and IWCMC. He received the Excellent Doctoral Dissertation Award from the Chinese Institute of Electronics, the Outstanding Ph.D. Graduate Award from Tsinghua University, the Excellent Doctoral Dissertation Award from Tsinghua University, National Scholarship, and the Academic Star of Electronic Engineering Department in Tsinghua University. He also serves as an Associate Editor for the IEEE Access.

JINLONG WEI received the Ph.D. degree in electronic engineering from Bangor University, Bangor, U.K., in 2010. He was a Post-Doctoral Researcher before joining the Centre for Photonics Systems, Cambridge University, U.K., as a Research Associate in 2011. He is currently a Senior Researcher with Huawei Düsseldorf GmbH, European Research Center, Germany. He was awarded the Marie Curie Fellowship and joined ADVA Optical Networking SE, Germany, as a Senior Engineer, in 2014. He has participated about 10 European national and international projects as well as projects with industry and realized a number of world-first system demonstrations with his colleagues. He has been contributing to the next generation 100 Gigabit Ethernet study within IEEE802.3. He has authored and co-authored over 120 journal and conference publications and five public patents.

QIXIANG CHENG received the B.S. degree from the Huazhong University of Science and Technology, China, in 2010, and the Ph.D. degree in III/V integrated optical switches from the University of Cambridge, U.K., in 2014. He has over 20 journal and conference publications. His current research interests include energy efficient data communications and optical switching.

TIANTIAN ZHANG received the B.S. degree from Qingdao Technological University in 2013. She is currently pursuing the Ph.D. degree with the State Key Laboratory of Information Photonics and Optical Communications, School of Information and Communication Engineering, Beijing University of Posts and Telecommunications. Her current research interests include visible light indoor localization and signal processing for optical orthogonal frequency-division multiplexing systems and optical wireless communications.

ZHANYU YANG received the B.S. degree in physics from Beijing Capital Normal University in 2010 and the M.S. degree from the State Key Laboratory of Information Photonics and Optical Communications, Beijing University of Posts and Telecommunications, China, in 2013. He is currently pursuing the Ph.D. degree in electrical and computer engineering with the University of Virginia. His research interests include high power photodiodes and their applications in analog links.

AIYING YANG received the B.S. degree in physics from Jilin University, China, in 1997, and the Ph.D. degree in information and communication system from Peking University in 2003. She is currently a Professor with the School of Optoelectronics, Beijing Institute of Technology, China. Her current research interests are in optical fiber communications and visible light communications.

YUEMING LU received the B.S. and M.S. degrees in computer science from the Xi'an University of Architecture and Technology in 1994 and 1997, respectively, and the Ph.D. degree in computer architecture from Xi'an Jiaotong University in 2000. He was a Researcher with the Optical Network Group Pacific for 10-Gb/s optical transportation networks at Lucent, from 2000 to 2003. He is currently a Professor with the Beijing University of Posts and Telecommunications, and he is also the Academic Committee Member of the Key Laboratory of Trustworthy Distributed Computing and Service, Ministry of Education.

YAOJUN QIAO received the B.S. degree from Hebei Normal University, Shijiazhuang, China, in 1994, the M.S. degree from Jilin University, Jilin, China, in 1997, and the Ph.D. degree from the Beijing University of Posts and Telecommunications, Beijing, China, in 2000. He was with Lucent and Fujitsu from 2000 to 2007. In 2007, he joined the Beijing University of Posts and Telecommunications. He is currently a Professor with the School of Information and Communication Engineering, Beijing University of Posts and Telecommunications. His research interests include optical and wireless communications.